THE JOURNAL OF PHYSICAL CHEMISTRY LETTERS
A JOURNAL OF THE AMERICAN CHEMICAL SOCIETY

pubs.acs.org/JPCL

Letter

Light Amplification in Fe-Doped $CsPbBr_3$ Crystal Microwire Excited by Continuous-Wave Laser

Shuangyang Zou,* Xiaoan Zhao, Jing Lyu, Wenze Ouyang, Ruibin Liu, and Shenghua Xu*

Cite This: *J. Phys. Chem. Lett.* 2023, 14, 4815−4821

Read Online

ACCESS | Metrics & More | Article Recommendations | Supporting Information

ABSTRACT: Electrically pumped halide perovskite laser diodes remain unexplored, and it is widely acknowledged that continuous-wave (CW) lasing will be a crucial step. Here, we demonstrate room-temperature amplified spontaneous emission of Fe-doped $CsPbBr_3$ crystal microwire excited by a CW laser. Temperature-dependent photoluminescence spectra indicate that the Fe dopant forms a shallow level trap states near the band edge of the lightly doped $CsPbBr_3$ microcrystal. Pump intensity-dependent time-resolved PL spectra show that the introduced Fe dopant level makes the electron more stable in excited states, suitable for the population inversion. The emission peak intensity of the lightly Fe-doped microwire increases nonlinearly above a threshold of 12.3 kW/cm^2 under CW laser excitation, indicating a significant light amplification. Under high excitation, the uniform crystal structure and surface outcoupling in Fe-doped perovskite crystal microwires enhanced the spontaneous emission. These results reveal the considerable promise of Fe-doped perovskite crystal microwires toward low-cost, high-performance, room-temperature electrical pumping perovskite lasers.

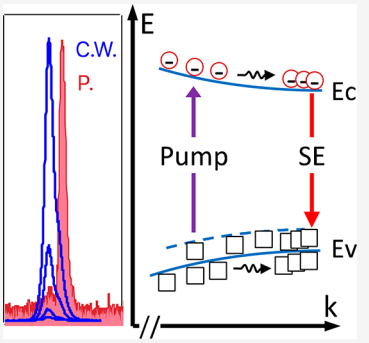

Amplified spontaneous emission (ASE) and lasing of micro/nanomaterials have been widely explored because of their tunable emission and gain wavelengths, high efficiency, and solution processability.[1,2] Among these, perovskites fulfill all these merits and have aroused much imagination as a gain medium for laser because of their excellent bandgap tunability, highly efficient optical gain, high defect tolerance, and simple solution synthesis.[3−14] High photoluminescence (PL) efficiency and optically pumped lasing have been demonstrated in halide perovskite semiconductors.[15] Since then, numerous studies have focused on decreasing the laser threshold, improving mode quality, feedback control, and increasing the stability of lead halide perovskites. However, despite the laser threshold going down to a few μJ/cm^2 and the quality factor increase to a few thousand,[16−18] most of the previously reported perovskite ASE and lasing with the Bragger reflector or distributed feedback structures are pumped by pulsed laser excitation, which is not suitable for the continuous carrier injection for electrically pumped laser. To change the optically pumping source into that electrically, it is necessary to study continuous-wave (CW) optically driven laser with perovskites, including hybrid organic−inorganic[19] and pure inorganic three-dimensional (3D) perovskites,[20] and perovskite with different shapes.[21] Remarkably, CW-pumped lasing has been achieved in one-dimensional (1D) cesium lead bromide perovskite nanowires[22] with a threshold of 6 kW/cm^2, compared with perovskite thin films[23,24] except for the low operating temperature (77 K). However, to realize commercial use, the critical issue of operating a 1D perovskite CW laser at room temperature should be addressed.

Optical gain is essential to produce a population inversion, which is fundamental for the semiconductor laser. All-inorganic lead halide perovskites have recently demonstrated their efficient population inversion properties at room temperature. At the same time, doping perovskite with extrinsic (aliovalent) ions is an efficient way to increase the charge carrier density of perovskite, which is a promising strategy for preparing highly efficient luminescence and stable optoelectronic devices.[25,26] What is more, long-lived population inversion and a lower threshold have also been demonstrated in doped nanomaterials.[27] Recently, we have successfully doped Fe into mixed halide perovskite bulk crystal $CsPb(Cl/Br)_3$ microwire, showing enhanced two-photon absorption (TPA) coefficient.[28] Fe ions in the lead halide perovskite lattice increase the charge density and quadrupole transition of the two-dimensional (2D) excitons in an anisotropic structure, resulting in an intensive light-matter interaction and high TPA. The well-defined cavity of the microwire could ensure constructive interference and allow specific modes to oscillate. Therefore, a doped crystal microwire is an ideal gain medium for ASE and further electrically pumped CW lasing, which could be realized potentially at low excitation thresholds at room temperature.

Received: January 30, 2023
Accepted: May 15, 2023
Published: May 16, 2023

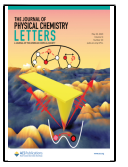

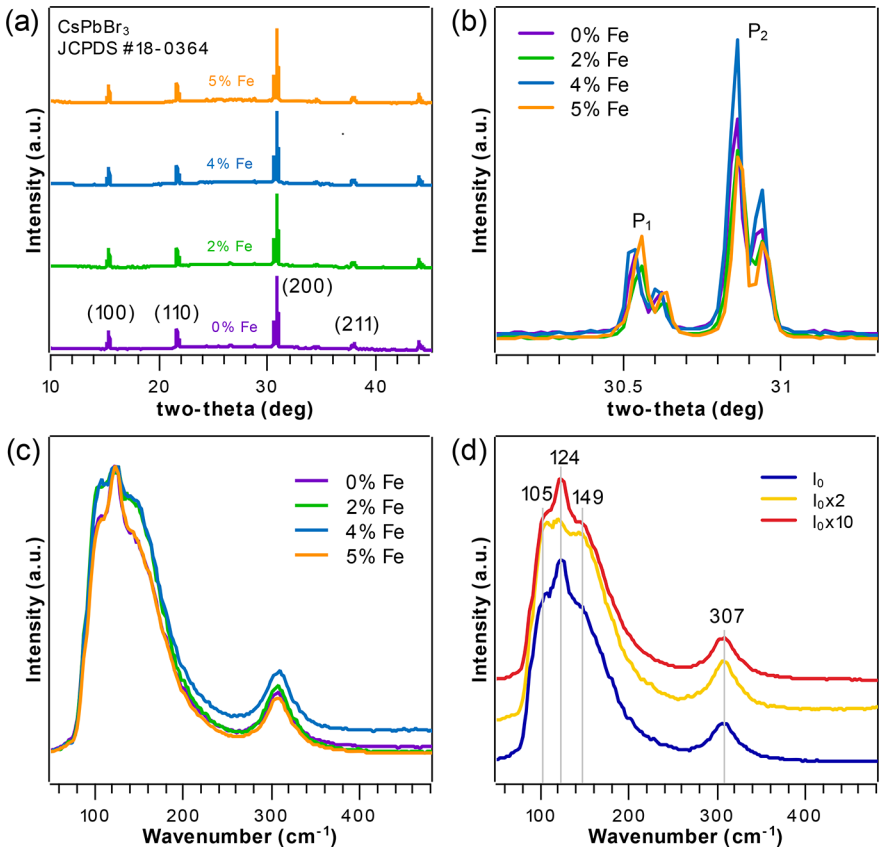

Figure 1. Powder X-ray diffraction patterns (a, b) and micro-Raman spectra (c, d) of synthesized $CsPbBr_3$ crystal microwire with different Fe dopant concentrations and excitation power dependence, respectively.

In this study, we demonstrate the ASE in Fe-doped $CsPbBr_3$ crystal microwires excited by CW laser at room temperature. The Fe-doped $CsPbBr_3$ crystal microwires were fabricated by a pressure-assisted antisolvent method. We investigated the photoluminescence (PL) of an Fe-doped $CsPbBr_3$ crystal microwire excited by a CW laser (405 nm) at room temperature. Consequently, we show that the PL intensity increases nonlinearly above a threshold of 12.3 kW/cm^2. These findings provide insights into the free carrier recombination in hole doping $CsPbBr_3$ microwires, which show the potential to be a promising gain medium for electrical pumping lasers.

The Fe-doped $CsPbBr_3$ crystal microwires were synthesized by the high-pressure antisolvent precipitation (HPAP) method.[28] Inspired by the well-known hydrothermal and antisolvent solution method, we put a small vial filled with a mixture of dimethyl sulfoxide (DMSO) solution of $PbBr_2$ and CsBr into a Teflon container (Figure S1, Supporting Information). After injecting ethanol antisolvent outside the vial, the Teflon container is fixed in the stainless steel autoclave and maintained in the oven at 100 °C for 10 h. Due to the intrinsically low formation energy and assistance of high-pressure, perovskite microwires successfully grow in solution on the bottom of the vial. More details of microwire synthesis are described in the experimental section in the Supporting Information. Since the Teflon-lined containers are sealed in a pressure vessel with high pressure and high temperature, it is still not possible to monitor the different growth stages from nanocrystal to microcrystal. The Fe-doped $CsPbBr_3$ microwires were synthesized when the appropriate iron bromide was added to the precursor $PbBr_2$ and CsBr before heating. After the reaction, the synthesized $CsPbBr_3$ crystal microwires were kept in a desiccator.

Powder X-ray diffraction (XRD) is the most efficient way to characterize the crystalline structure of materials. For the Fe-doped $CsPbBr_3$ microwire, three different amounts of $FeBr_3$ (2, 4, and 5 mol %, respectively) were added to the mixture solution of $PbBr_2$ and CsBr. As shown in Figure 1a, the XRD patterns of the $CsPbBr_3$ microwires have three prominent diffraction peaks at (100) (110) (200). These sharp peaks indicate that the microwires are crystalline and consistent with the monoclinic structure in the previous reports.[29,30] The dopant Fe concentration could be tiny in the microwire, which has been quantitatively analyzed by electron probe micro-analysis (EPMA) (Table S1, Supporting Information). Since no microwires have been obtained in the stainless steel autoclave at room temperature, we considered that the temperature-induced higher pressure facilitates the growth of perovskite microwires. Figure 1b shows the selected area of the diffraction peak of Fe-doped microwires from Figure 1a. The relation between peaks (P_1, P_2) and dopant concentration is described in Figure S2a. Generally, the intensity of X-ray scattering is proportional to the square of the structure factor ($I_{(hkl)} \propto |S_{(hkl)}|^2$). The relatively small radius of Fe ion dopant in perovskite may cause structure factor changes, further reflected in the X-ray diffraction peak. The peak (200) position shift may occur due to the presence of Fe ions in the structure of $CsPbBr_3$ or because of lattice strain due to the mismatch in lattice parameters of the microwire surface.

Raman spectroscopy is a reliable probe for exploring the local chemical structure by measuring the vibrational modes of

https://doi.org/10.1021/acs.jpclett.3c00277
J. Phys. Chem. Lett. 2023, 14, 4815−4821

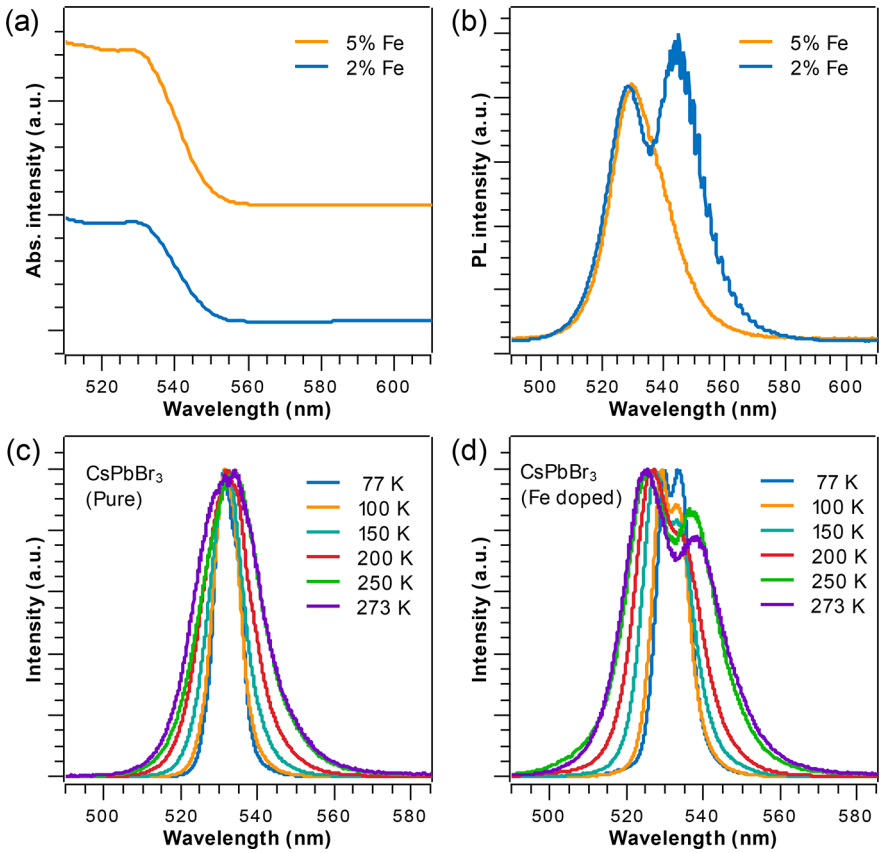

Figure 2. Absorption (a) and PL (b) spectra of a representative Fe-doped lead halide perovskite microwire. Temperature-dependent PL spectra of pure (c) and lightly Fe-doped (d) $CsPbBr_3$ microwire.

a material, which could provide detailed vibrational modes of the metal halide sublattice. As for the $CsPbBr_3$ crystal structure, the Cs^+ cation is located in the octahedral spaces between the corner-sharing octahedra of $PbBr_6^-$. Figure 1c shows the room-temperature Raman spectra of the $CsPbBr_3$ microwire with different Fe dopant concentrations (0%, 2%, 4%, and 5% Fe) at an excitation wavelength of 633 nm. More doped samples are shown in Figure S2b. The overall profiles of the Raman spectral features between various concentrations of Fe dopants in the microwire are similar. The heavily doped microwire (5% Fe) has shown almost the same Raman profile as the pure microwire. However, there is an apparent difference, in the range between ∼80 and ∼200 cm^{-1}, of Raman peak for lightly doped microwire (2% and 4% Fe). The quickly grown perovskite crystals may cause the removal of dopant ions under heavily doped conditions.

Figure 1d shows the power-dependent Raman spectra of the doped $CsPbBr_3$ microwire. The spectra under different excitation intensities are offset for clarity. There is almost no peak position shift in Raman spectra without regard to relative intensity, revealing the good crystal stability of the $CsPbBr_3$ microwire. The vibrational mode at 124 cm^{-1} (16 meV) is associated with movements of the Cs^+ cation and $PbBr_6^-$ octahedral modes, related to the transverse optical phonon mode. The peak at ∼149 cm^{-1} is associated with the longitudinal optical (LO) phonon of the Pb−Br stretching mode in a $CsPbBr_3$ crystal. The prominent Raman modes at 105, 124, and 149 cm^{-1}, a broad overlapping peak in the Raman spectra, indicate the asymmetric and symmetric bending modes of Pb−Br octahedra combining with transverse optical phonon and LO phonon.[31,32] With the assistance of the prominent optical phonon, the charge carrier could be modified during excitation, diffusion, and the radiative transition.[33] These phonon modes could couple to photo-generated charge carriers and increase their long-range interaction via large polaron formation.[34] The mode at 305 cm^{-1} may be assigned to a second-order vibrational mode associated with the translation motion of the Cs^+ cation.[35] The significant intensity of peaks at ∼124 and 305 cm^{-1} can serve as indicators of a perovskite microwire made from HPAP. The LO phonon position at 149 cm^{-1} (19 meV) is typically larger than that of organic hybrid lead halide perovskites.[36] There is no noticeable peak position change compared with that of the host crystal structure. The Fe-doped inorganic lead halide perovskite microwire shows good structural stability during measurement, even though the dopant concentration is up to 5%.

The good stability of the crystal structure and successful doping of Fe in the $CsPbBr_3$ crystal microwire allow the investigation of PL properties. Figure 2a shows the representative absorption spectrum of two representative different Fe-doped perovskite microwires bunched on the glass substrate. An absorption edge exists around 550 nm (2.3 eV) at room temperature.

Moreover, a narrow excitonic absorption peak at 529 nm shows a stable exciton binding energy. The lightly Fe-doped perovskite does not change the bandgap of the bulk crystal. The PL spectra of the microwire with a wide range of dopant concentrations are demonstrated in Figure S3. Figure 2b shows the two representative micro-PL spectra of the Fe-doped single

https://doi.org/10.1021/acs.jpclett.3c00277
J. Phys. Chem. Lett. 2023, 14, 4815−4821

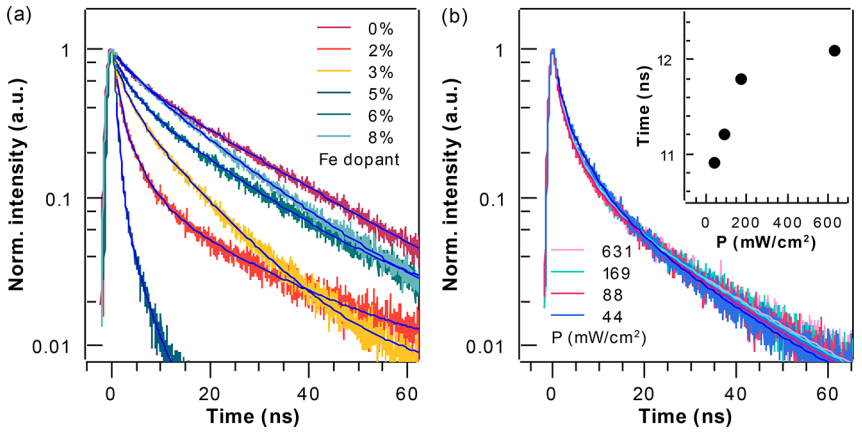

Figure 3. Time-resolved PL of Fe-doped microwire. (a) Fe doping concentration is from 2% to 8%. (b) Pump intensity dependent time-resolved PL of an Fe-doped microcrystal (3%).

microwire. The near-band-edge (NBE) emission of one-dimensional $CsPbBr_3$ is around 530 nm.[16] A remarkable multipeak emission was detected in lightly doped microwire (2−3%) but not in heavily doped microwire (5−9%), which can be attributed to a Fabry−Perot mode emission coming from the dopant energy level in uniform morphology of the microwire.[37] The lightly Fe-doped microwire can confine photons between the opposite facets and establish Fabry−Perot modes. These multiple PL peaks at a longer wavelength come from the combination of photon reabsorption, reflection, and resonance emission.[38] The Fe dopant could form a dopant level and trap the electron near the bottom of the conduction band (E_c) in the lightly doped $CsPbBr_3$ microcrystal, which shows a trap state emission at a longer wavelength. Moreover, temperature-dependent PL spectra of pure microwire and Fe-doped microwire are demonstrated in Figure 2c,d. The full width at half maximum (FWHM) of emission peaks is narrowing (<8 nm) at liquid nitrogen temperature (77 K), indicating a decrease of electron−phonon coupling and suppression of nonradiative recombination.

The typical time-resolved PL (TRPL) of the Fe-doped $CsPbBr_3$ crystal microwire was measured using the time-correlated single photon counting (TCSPC) technique. Figure 3a shows the PL lifetime of the microwire at different Fe dopant concentrations. The PL lifetime was fitted by the exponential decay function $y = A_1 \exp(-t/\tau_1) + A_2 \exp(-t/\tau_2) + y_0$, where the PL decay traces can be fitted to determine the fast (τ_1) and slow (τ_2) components of the PL decay. At the same excitation power (0.6 W/cm^2), microwire with a high dopant concentration (>5%) shows a relatively slow decay time compared with that of a low dopant concentration (<5%). The average PL lifetimes of different doping concentrations are 10−20 ns (Table S2). The PL lifetime of doping concentration (5%) after biexponential decay fitting is ∼2 ns, corresponding to a short carrier recombination time. The probably dangling bonds and surface defects lead to fast nonradiative surface recombination, resulting in a faster lifetime. In Figure 3b, the pump intensity-dependent PL decay profile of doped crystal shows a longer PL lifetime with increasing pump intensity, which indicates that the introduced Fe dopant level makes the carrier longer lifetime in excited states. The corresponding average PL lifetimes are shown in Table S3. The heavily doped (Fe) in bulk microwire crystal generates high carrier density, larger scattering cross-section, which finally increases the ratio of a longer lifetime.[39,40] The representative fluorescence lifetime images (FLIMs) of two microwires corresponding to TRPL are shown in Figure S4. Point defects (doping) could significantly change the carrier concentration and increase the carrier lifetime by forming large polarons. The delocalized large polarons formed in a relatively lightly doped $CsPbBr_3$ crystal microwire with a substitution of Fe ions doping in the crystal lattice, which shows weak coupling and long-range interaction, and form a coherent transition behavior under the CW excitation. We, therefore, choose the lightly doped microwires (3%) for the following excitation power-dependent PL.

The PL intensity as a function of excitation intensity in a lightly doped single microwire (3%) is plotted in Figure 4a,b

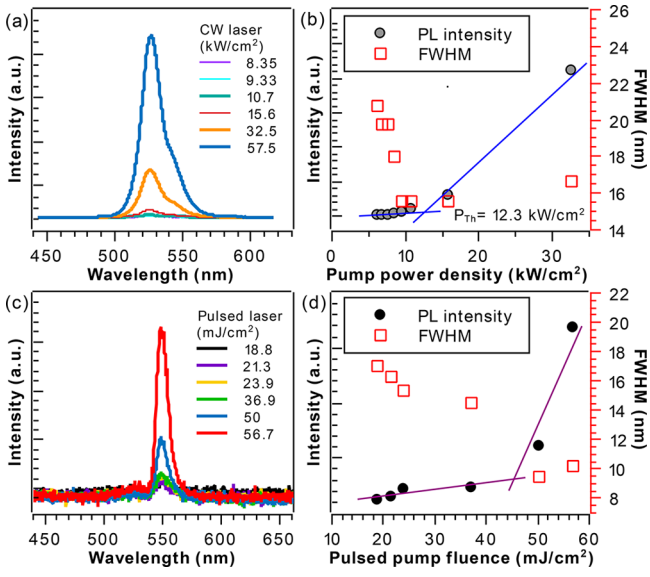

Figure 4. PL spectra of the lightly Fe-doped $CsPbBr_3$ crystal microwire by CW laser (a) and pulsed laser (c). The relationship between emission peak and excitation is shown in (b) and (d).

under the CW 405 nm laser excitation. The corresponding interval time is the same for different excitation intensities during measurements. First, at the low excitation intensity (<12.3 kW/cm^2), PL intensity increases linearly, indicating a well-known spontaneous emission. As the excitation intensity increases (>12.3 kW/cm^2), the PL intensity increases super-linearly, which presents a typical threshold. The Fe dopant in the $CsPbBr_3$ host could trap free carriers and the coupling with

https://doi.org/10.1021/acs.jpclett.3c00277
J. Phys. Chem. Lett. 2023, 14, 4815−4821

phonon. A sufficiently large number of electrons produces a population inversion transition from an excited state to the ground state, making the spontaneous emission amplified. The peak position remains stable during light amplification, indicating good crystal structure and emission stability. PL intensities and FWHM dependence of different doped microwires on excitation intensities are shown in Figure S5. The FWHM of the emission peak is a little broad (~16 nm) even with high intensity, which is highly related to the feedback to provide phase coherence and the thermal effect from the CW laser for a long interaction time. The crystal surface damage occurs when excitation intensity increases to hundreds of kW/cm^2. The excitation-induced surface degradation of microwire crystals at high pump power can further increase outcoupling and lead to superlinear emission.

During CW laser excitation, the radiative recombination of bound excitons is coupled by various acoustic phonon absorptions and emissions that could broaden the PL emission[36] at room temperature, which limits exciton mobilities and impedes the emission line narrowing. At low temperatures, these carriers are less scattered by the phonon and photon excitations, and the FWHM of the emission peak becomes narrower, as shown in Figure 2c,d. Since pulsed laser induces significantly higher excitation power density (~MW/cm^2) than CW laser, thousands of orders larger, the FWHM of PL emission of microwire excited by ns pulsed 355 nm laser could decrease to several nm (~9 nm) accompanying with PL intensity nonlinearly increasing (Figure 4c,d). Much less phonon scattered during emission under pulsed excitation, which could account for the low FWHM of the microwire.

For comparison, we measured the PL intensity of the quantum dots (QDs) polymer composites as a function of the excitation intensity. Although the PL intensity increases nonlinearly as excitation intensity increases, it does not show an apparent threshold (Figure S6). The trap-assisted Auger nonradiative recombination losses and charge transport in QDs ligands may hinder the threshold occurring.[41,42]

In summary, we have demonstrated the significant light amplification in Fe-doped $CsPbBr_3$ crystal microwire excited by a continuous-wave laser at room temperature. One-dimensional Fe-doped $CsPbBr_3$ microwire was fabricated via the HPAP method suitable for perovskite microcrystal growth. XRD and Raman spectra show that perovskite microwires have monoclinic structures with the transverse optical phonon (~16 meV) and LO phonon (~19 meV) modes of the Cs^+ cation and $PbBr_6^-$ octahedral vibration. The absorbance and PL of the Fe-doped $CsPbBr_3$ crystal microwire indicate a direct bandgap of about ~2.3 eV. Temperature-dependent PL spectra indicate that a large number of optical phonons scattered in Fe-doped crystal during emission, indicating multiple excitations could broaden the FWHM at room temperature. Excitation-intensity dependent time-resolved PL of the Fe-doped crystal microwire indicates that lightly doping with Fe could increase charge carrier densities and induce trap states, stabilizing more carriers in excited states under high excitation intensity, which is beneficial for the population inversion. We then investigated the excitation-intensity dependent PL spectra of Fe-doped $CsPbBr_3$ perovskite single microwire under the CW laser pump at room temperature, which shows the PL peak intensity increases superlinearly above a threshold (12.3 kW/cm^2). The extraordinary ASE of Fe-doped $CsPbBr_3$ microwires may serve as a potential gain medium for electrical pumping laser, and the perovskite microwire laser diode is promising for developing the next-generation highly integrated photonic/optoelectronic systems.

■ ASSOCIATED CONTENT

Supporting Information

The Supporting Information is available free of charge at https://pubs.acs.org/doi/10.1021/acs.jpclett.3c00277.

Details of experimental methods: Schematic illustration of perovskite microwires synthesis, Raman spectra of Fe-doped microwires, Electron probe analysis, Scanning electron microscopic image, Fluorescence lifetime images, Excitation power-dependent PL spectra of QDs composite, Optical photograph of microcrystal (PDF)

■ AUTHOR INFORMATION

Corresponding Authors

Shuangyang Zou − *Key Laboratory of Microgravity, Institute of Mechanics, Chinese Academy of Sciences, Beijing 100190, China;* orcid.org/0000-0002-5519-8865; Email: shuangyang.zou@imech.ac.cn

Shenghua Xu − *Key Laboratory of Microgravity, Institute of Mechanics, Chinese Academy of Sciences, Beijing 100190, China; School of Engineering Science, University of Chinese Academy of Sciences, Beijing 100149, China;* orcid.org/0000-0001-5433-0409; Email: xush@imech.ac.cn

Authors

Xiaoan Zhao − *Key Laboratory of Microgravity, Institute of Mechanics, Chinese Academy of Sciences, Beijing 100190, China; School of Engineering Science, University of Chinese Academy of Sciences, Beijing 100149, China*

Jing Lyu − *Beijing Key Lab of Nano-photonics and Ultrafine Optoelectronic Systems, Beijing Institute of Technology, Beijing 100081, China*

Wenze Ouyang − *Key Laboratory of Microgravity, Institute of Mechanics, Chinese Academy of Sciences, Beijing 100190, China*

Ruibin Liu − *Beijing Key Lab of Nano-photonics and Ultrafine Optoelectronic Systems, Beijing Institute of Technology, Beijing 100081, China;* orcid.org/0000-0002-7507-9126

Complete contact information is available at: https://pubs.acs.org/10.1021/acs.jpclett.3c00277

Notes

The authors declare no competing financial interest.

■ ACKNOWLEDGMENTS

This work was financially supported by the National Natural Science Foundation of China (Grant Nos. 22172180, 22272191). We thank Yifan Wang from the Institute of Process Engineering, Chinese Academy of Sciences, for the EPMA measurement of Fe-doped $CsPbBr_3$ microwires. We especially thank Prof. Heng Lu from the Technical Institute of Physics and Chemistry, Chinese Academy of Sciences, for the discussion and TRPL measurements. We also thank Dr. Duan Zhao and Dr. Shilong Li from the Institute of Physics, Chinese Academy of Sciences, for arranging the temperature-dependent PL measurement of Fe-doped $CsPbBr_3$ microwires.

REFERENCES

(1) She, C.; Fedin, I.; Dolzhnikov, D. S.; Dahlberg, P. D.; Engel, G. S.; Schaller, R. D.; Talapin, D. v. Red, Yellow, Green, and Blue Amplified Spontaneous Emission and Lasing Using Colloidal CdSe Nanoplatelets. *ACS Nano* **2015**, *9* (10), 9475−9485.

(2) Zhang, W.; Yao, J.; Zhao, Y. S. Organic Micro/Nanoscale Lasers. *Acc. Chem. Res.* **2016**, *49* (9), 1691−1700.

(3) Sutherland, B. R.; Sargent, E. H. Perovskite Photonic Sources. *Nat. Photonics* **2016**, *10* (5), 295−302.

(4) Wang, K.; Wang, S.; Xiao, S.; Song, Q. Recent Advances in Perovskite Micro- and Nanolasers. *Adv. Opt Mater.* **2018**, *6* (18), 1800278.

(5) Xing, G.; Mathews, N.; Lim, S. S.; Yantara, N.; Liu, X.; Sabba, D.; Grätzel, M.; Mhaisalkar, S.; Sum, T. C. Low-Temperature Solution-Processed Wavelength-Tunable Perovskites for Lasing. *Nat. Mater.* **2014**, *13* (5), 476−480.

(6) Yakunin, S.; Protesescu, L.; Krieg, F.; Bodnarchuk, M. I.; Nedelcu, G.; Humer, M.; de Luca, G.; Fiebig, M.; Heiss, W.; Kovalenko, M. V. Low-Threshold Amplified Spontaneous Emission and Lasing from Colloidal Nanocrystals of Caesium Lead Halide Perovskites. *Nat. Commun.* **2015**, *6* (1), 8056.

(7) Zhang, F.; Zhong, H.; Chen, C.; Wu, X. G.; Hu, X.; Huang, H.; Han, J.; Zou, B.; Dong, Y. Brightly Luminescent and Color-Tunable Colloidal $CH_3NH_3PbX_3$ (X = Br, I, Cl) Quantum Dots: Potential Alternatives for Display Technology. *ACS Nano* **2015**, *9* (4), 4533−4542.

(8) Zhang, P.; Yang, G.; Li, F.; Shi, J.; Zhong, H. Direct in Situ Photolithography of Perovskite Quantum Dots Based on Photocatalysis of Lead Bromide Complexes. *Nat. Commun.* **2022**, *13* (1), 6713.

(9) Ma, W.; Ding, C.; Wazir, N.; Wang, X.; Kong, D.; Li, A.; Zou, B.; Liu, R. Enhancing the Photo-Luminescence Stability of $CH_3NH_3PbI_3$ Film with Ionic Liquids. *Chinese Phys. B* **2022**, *31* (3), 037802.

(10) Ren, M.; Cao, S.; Zhao, J.; Zou, B.; Zeng, R. Advances and Challenges in Two-Dimensional Organic−Inorganic Hybrid Perovskites Toward High-Performance Light-Emitting Diodes. *Nanomicro Lett.* **2021**, *13* (1), 163.

(11) Zeng, R.; Zhang, L.; Xue, Y.; Ke, B.; Zhao, Z.; Huang, D.; Wei, Q.; Zhou, W.; Zou, B. Highly Efficient Blue Emission from Self-Trapped Excitons in Stable Sb^{3+} -Doped $Cs_2NaInCl_6$ Double Perovskites. *J. Phys. Chem. Lett.* **2020**, *11* (6), 2053−2061.

(12) Chen, C.; Zhang, S.; Zeng, R.; Luo, B.; Chen, Y.; Cao, S.; Zhao, J.; Zou, B.; Zhang, J. Z. Competing Energy Transfer in Two-Dimensional Mn $^{2+}$ -Doped $BDACdBr_4$ Hybrid Layered Perovskites with Near-Unity Photoluminescence Quantum Yield. *ACS Appl. Mater. Interfaces* **2022**, *14* (40), 45725−45733.

(13) Zeng, R.; Bai, K.; Wei, Q.; Chang, T.; Yan, J.; Ke, B.; Huang, J.; Wang, L.; Zhou, W.; Cao, S.; Zhao, J.; Zou, B. Boosting Triplet Self-Trapped Exciton Emission in Te(IV)-Doped Cs_2SnCl_6 Perovskite Variants. *Nano Res.* **2021**, *14* (5), 1551−1558.

(14) Sheng, Y.; Chen, W.; Hu, F.; Liu, C.; Di, Y.; Sheng, C.; Chen, Z.; Jia, B.; Wen, X.; Gan, Z. Mechanism of Photoinduced Phase Segregation in Mixed-Halide Perovskite Microplatelets and Its Application in Micropatterning. *ACS Appl. Mater. Interfaces* **2022**, *14* (10), 12412−12422.

(15) Deschler, F.; Price, M.; Pathak, S.; Klintberg, L. E.; Jarausch, D.-D.; Higler, R.; Hüttner, S.; Leijtens, T.; Stranks, S. D.; Snaith, H. J.; Atatüre, M.; Phillips, R. T.; Friend, R. H. High Photoluminescence Efficiency and Optically Pumped Lasing in Solution-Processed Mixed Halide Perovskite Semiconductors. *J. Phys. Chem. Lett.* **2014**, *5* (8), 1421−1426.

(16) Wang, X.; Shoaib, M.; Wang, X.; Zhang, X.; He, M.; Luo, Z.; Zheng, W.; Li, H.; Yang, T.; Zhu, X.; Ma, L.; Pan, A. High-Quality In-Plane Aligned $CsPbX_3$ Perovskite Nanowire Lasers with Composition-Dependent Strong Exciton−Photon Coupling. *ACS Nano* **2018**, *12* (6), 6170−6178.

(17) Zhu, H.; Fu, Y.; Meng, F.; Wu, X.; Gong, Z.; Ding, Q.; Gustafsson, M. v.; Trinh, M. T.; Jin, S.; Zhu, X.-Y. Lead Halide Perovskite Nanowire Lasers with Low Lasing Thresholds and High Quality Factors. *Nat. Mater.* **2015**, *14* (6), 636−642.

(18) Su, R.; Wang, J.; Zhao, J.; Xing, J.; Zhao, W.; Diederichs, C.; Liew, T. C. H.; Xiong, Q. Room Temperature Long-Range Coherent Exciton Polariton Condensate Flow in Lead Halide Perovskites. *Sci. Adv.* **2018**, *4* (10), No. eaau0244.

(19) Jia, Y.; Kerner, R. A.; Grede, A. J.; Rand, B. P.; Giebink, N. C. Continuous-Wave Lasing in an Organic-Inorganic Lead Halide Perovskite Semiconductor. *Nat. Photonics* **2017**, *11* (12), 784−788.

(20) Shang, Q.; Li, M.; Zhao, L.; Chen, D.; Zhang, S.; Chen, S.; Gao, P.; Shen, C.; Xing, J.; Xing, G.; Shen, B.; Liu, X.; Zhang, Q. Role of the Exciton−Polariton in a Continuous-Wave Optically Pumped $CsPbBr_3$ Perovskite Laser. *Nano Lett.* **2020**, *20* (9), 6636−6643.

(21) Su, R.; Diederichs, C.; Wang, J.; Liew, T. C. H.; Zhao, J.; Liu, S.; Xu, W.; Chen, Z.; Xiong, Q. Room-Temperature Polariton Lasing in All-Inorganic Perovskite Nanoplatelets. *Nano Lett.* **2017**, *17* (6), 3982−3988.

(22) Evans, T. J. S.; Schlaus, A.; Fu, Y.; Zhong, X.; Atallah, T. L.; Spencer, M. S.; Brus, L. E.; Jin, S.; Zhu, X.-Y. Continuous-Wave Lasing in Cesium Lead Bromide Perovskite Nanowires. *Adv. Opt Mater.* **2018**, *6* (2), 1700982.

(23) Brenner, P.; Bar-On, O.; Jakoby, M.; Allegro, I.; Richards, B. S.; Paetzold, U. W.; Howard, I. A.; Scheuer, J.; Lemmer, U. Continuous Wave Amplified Spontaneous Emission in Phase-Stable Lead Halide Perovskites. *Nat. Commun.* **2019**, *10* (1), 988.

(24) Qin, C.; Sandanayaka, A. S. D.; Zhao, C.; Matsushima, T.; Zhang, D.; Fujihara, T.; Adachi, C. Stable Room-Temperature Continuous-Wave Lasing in Quasi-2D Perovskite Films. *Nature* **2020**, *585* (7823), 53−57.

(25) Zhou, Y.; Chen, J.; Bakr, O. M.; Sun, H.-T. Metal-Doped Lead Halide Perovskites: Synthesis, Properties, and Optoelectronic Applications. *Chem. Mater.* **2018**, *30* (19), 6589−6613.

(26) Euvrard, J.; Yan, Y.; Mitzi, D. B. Electrical Doping in Halide Perovskites. *Nat. Rev. Mater.* **2021**, *6*, 531−549.

(27) Lahad, O.; Meir, N.; Pinkas, I.; Oron, D. Long-Lived Population Inversion in Isovalently Doped Quantum Dots. *ACS Nano* **2015**, *9* (1), 817−824.

(28) Zou, S.; Yang, G.; Yang, T.; Zhao, D.; Gan, Z.; Chen, W.; Zhong, H.; Wen, X.; Jia, B.; Zou, B. Template-Free Synthesis of High-Yield Fe-Doped Cesium Lead Halide Perovskite Ultralong Microwires with Enhanced Two-Photon Absorption. *J. Phys. Chem. Lett.* **2018**, *9* (17), 4878−4885.

(29) Jathar, S. B.; Rondiya, S. R.; Bade, B. R.; Nasane, M. P.; Barma, S. v.; Jadhav, Y. A.; Rokade, A. v.; Kore, K. B.; Nilegave, D. S.; Tandale, P. U.; Jadkar, S. R.; Funde, A. M. Facile Method for Synthesis of $CsPbBr_3$ Perovskite at Room Temperature for Solar Cell Applications. *ES Materials & Manufacturing* **2021**, *12*, 72−77.

(30) Liu, X.; Bai, R.; Guo, Z.; Che, Y.; Guo, C.; Xing, H. Photogeneration of Thiyl Radicals Using Metal-halide Perovskite for Highly Efficient Synthesis of Thioethers. *Appl. Organomet. Chem.* **2022**, *36* (2), No. e6492.

(31) Lao, X.; Yang, Z.; Su, Z.; Bao, Y.; Zhang, J.; Wang, X.; Cui, X.; Wang, M.; Yao, X.; Xu, S. Anomalous Temperature-Dependent Exciton−Phonon Coupling in Cesium Lead Bromide Perovskite Nanosheets. *J. Phys. Chem. C* **2019**, *123* (8), 5128−5135.

(32) Reuveni, G.; Diskin-Posner, Y.; Gehrmann, C.; Godse, S.; Gkikas, G. G.; Buchine, I.; Aharon, S.; Korobko, R.; Stoumpos, C. C.; Egger, D. A.; Yaffe, O. Static and Dynamic Disorder in Formamidinium Lead Bromide Single Crystals. *J. Phys. Chem. Lett.* **2023**, *14*, 1288.

(33) Zhang, Q.; Liu, X.; Utama, M. I. B.; Xing, G.; Sum, T. C.; Xiong, Q. Phonon-Assisted Anti-Stokes Lasing in ZnTe Nanoribbons. *Adv. Mater.* **2016**, *28* (2), 276−283.

(34) Miyata, K.; Meggiolaro, D.; Trinh, M. T.; Joshi, P. P.; Mosconi, E.; Jones, S. C.; de Angelis, F.; Zhu, X.-Y. Large Polarons in Lead Halide Perovskites. *Sci. Adv.* **2017**, *3* (8), No. e1701217.

(35) Naqvi, F. H.; Ko, J.-H.; Kim, T. H.; Ahn, C. W.; Hwang, Y.; Sheraz, M.; Kim, S. A-Site Cation Effect on Optical Phonon Modes and Thermal Stability in Lead-Based Perovskite Bromide Single

https://doi.org/10.1021/acs.jpclett.3c00277
J. Phys. Chem. Lett. 2023, 14, 4815−4821

Crystals Using Raman Spectroscopy. *J. Korean Phys. Soc.* **2022**, *81* (3), 230−240.
(36) Wright, A. D.; Verdi, C.; Milot, R. L.; Eperon, G. E.; Pérez-Osorio, M. A.; Snaith, H. J.; Giustino, F.; Johnston, M. B.; Herz, L. M. Electron−Phonon Coupling in Hybrid Lead Halide Perovskites. *Nat. Commun.* **2016**, *7* (1), 11755.
(37) Zhao, Z.; Zhong, M.; Zhou, W.; Peng, Y.; Yin, Y.; Tang, D.; Zou, B. Simultaneous Triplet Exciton−Phonon and Exciton−Photon Photoluminescence in the Individual Weak Confinement $CsPbBr_3$ Micro/Nanowires. *J. Phys. Chem. C* **2019**, *123* (41), 25349−25358.
(38) Pan, A.; Wang, X.; He, P.; Zhang, Q.; Wan, Q.; Zacharias, M.; Zhu, X.; Zou, B. Color-Changeable Optical Transport through Se-Doped CdS 1D Nanostructures. *Nano Lett.* **2007**, *7* (10), 2970−2975.
(39) Wehrenfennig, C.; Eperon, G. E.; Johnston, M. B.; Snaith, H. J.; Herz, L. M. High Charge Carrier Mobilities and Lifetimes in Organolead Trihalide Perovskites. *Adv. Mater.* **2014**, *26* (10), 1584−1589.
(40) Qin, J.; Liu, X.-K.; Yin, C.; Gao, F. Carrier Dynamics and Evaluation of Lasing Actions in Halide Perovskites. *Trends Chem.* **2021**, 3 (1), 34−46.
(41) Dang, C.; Lee, J.; Breen, C.; Steckel, J. S.; Coe-Sullivan, S.; Nurmikko, A. Red, Green and Blue Lasing Enabled by Single-Exciton Gain in Colloidal Quantum Dot Films. *Nat. Nanotechnol* **2012**, *7* (5), 335−339.
(42) Xue, J.; Wang, R.; Yang, Y. The Surface of Halide Perovskites from Nano to Bulk. *Nat. Rev. Mater.* **2020**, *5* (11), 809−827.

https://doi.org/10.1021/acs.jpclett.3c00277
J. Phys. Chem. Lett. 2023, 14, 4815−4821